Magnetic resonance and ultrasound image-guided navigation system using a needle manipulator

Short running title: Multi-modal image-guided navigation

Atsushi Yamada, PhD [1)], Junichi Tokuda, PhD [2)], Shigeyuki Naka, MD PhD [3)], Koichiro Murakami, MD, PhD [3)], Tohru Tani, MD PhD [1)], Shigehiro Morikawa, MD PhD [4)]

1) *Department of Research and Development for Innovative Medical Devices and Systems, Shiga University of Medical Science, Seta Tsukinowa-cho, Otsu, Shiga 520-2192, Japan*
2) *National Center for Image Guided Therapy, Brigham and Women's Hospital and Harvard Medical School, Boston, Massachusetts 02115, USA*
3) *Department of Surgery, Shiga University of Medical Science, Seta Tsukinowa-cho, Otsu, Shiga, 520-2192, Japan*
4) *Molecular Neuroscience Research Center, Shiga University of Medical Science, Seta Tsukinowa-cho, Otsu, Shiga 520-2192, Japan*

Corresponding author:
Atsushi Yamada, PhD
Department of Research and Development for Innovative Medical Devices and Systems, Shiga University of Medical Science, Seta Tsukinowa-cho, Otsu, Shiga 520-2192, Japan
Tel: +81-77-548-2345, Fax: +81-77-548-2132
E-mail: ayamada@belle.shiga-med.ac.jp

ABSTRACT

Purpose: Image guidance is crucial for percutaneous tumor ablations, enabling accurate needle-like applicator placement into target tumors while avoiding tissues that are sensitive to injury and/or correcting needle deflection. Although ultrasound (US) is widely used for image guidance, magnetic resonance (MR) is preferable due to its superior soft tissue contrast. The objective of this study was to develop and evaluate an MR and US multi-modal image-guided navigation system with a needle manipulator to enable US-guided applicator placement during MRI-guided percutaneous tumor ablation.

Methods: The MRI-compatible needle manipulator with US probe was installed adjacent to a 3 Tesla MRI scanner patient table. Coordinate systems for the MR image, patient table, manipulator, and US probe were all registered using an optical tracking sensor. The patient was initially scanned in the MRI scanner bore for planning and then moved outside the bore for treatment. Needle insertion was guided by real-time US imaging fused with the reformatted static MR image to enhance soft tissue contrast. Feasibility, targeting accuracy, and MR compatibility of the system were evaluated using a bovine liver and agar phantoms.

Results: Targeting error for 50 needle insertions was 1.6 ± 0.6 mm (mean ± standard deviation). The experiment confirmed that fused MR and US images provided real-time needle localization against static MR images with soft tissue contrast.

Conclusions: The proposed MR and US multi-modal image-guided navigation system using a needle manipulator enabled accurate needle insertion by taking advantage of static MR and real-time US images simultaneously. Real-time visualization helped determine needle depth,

47 tissue monitoring surrounding the needle path, target organ shifts, and needle deviation
48 from the path.

49 **Key words**: medical robot, magnetic resonance imaging, image-guided therapy, liver
50 ablation

51

1. INTRODUCTION

Percutaneous tumor ablations, such as ethanol injection, cryotherapy, laser interstitial thermal therapy, radiofrequency ablation, and microwave coagulation therapy are widely performed for patients who are not candidates for surgical resection[1–3]. Those procedures are often performed under image guidance to place needle-like applicators into target tumors accurately while avoiding tissues that may be sensitive to injury and/or correcting needle deflections. Image guidance is particularly important when a target organ is moving due to respiration. Although ultrasonography and computed tomography (CT) are commonly employed, intra-procedural magnetic resonance imaging (MRI) has also been investigated[4,5] due to its superior soft tissue contrast. One technical challenge for intra-procedural MRI is to allow the physician to interactively maneuver the needle under real-time image guidance because conventional closed-bore MRI inhibits the physician from accessing the treated area.

We previously developed a real-time MRI-guided navigation system[6–8] dedicated for a 0.5 Tesla (T) vertical open-configuration MRI scanner (Signa SP/2, GE Healthcare, Milwaukee, WI) [9]. This navigation system leveraged the unique scanner configuration, allowing physicians to access the patient in the bore during scanning, and hence enabling interactive planning and targeting using a handheld needle guide[10,11]. This system was subsequently successfully employed for microwave ablations of liver tumors in more than 300 clinical cases from 2000 to 2016[6–8,12–14]. We recently developed an MRI-compatible cooperative needle manipulator[15] to replace the handheld needle guide, providing more interactive and accurate targeting, and successfully clinically tested this system for 23 ablation cases[16]. The study demonstrated that the physical assistance provided by the

cooperative needle manipulator improved targeting interactivity under MRI guidance and helped reduce trial-and-error attempts before reaching the target. However, the manipulator is incompatible with conventional closed-bore MRI scanners because its mechanical configuration and clinical workflow are highly dependent on the specific open-configuration MRI scanner.

The goal of this study was to enable the physician to interactively maneuver a needle under MRI guidance for percutaneous tumor ablation using a widely available closed-bore MRI scanner. To achieve this, we developed a multi-modal image-guided navigation system where needle placement occurs outside the MRI scanner under MRI–ultrasound (US) fusion guidance combined with physical assistance provided by the needle manipulator. The system adapted an "in/scan-out/adjust technique"[17] where the patient was scanned in the bore for planning and then moved out for needle placement and adjustment. The manipulator was equipped with a US probe to provide real-time image feedback during needle insertion. The navigation system could also visualize multiplanar reconstructed (MPR) MR images with sections synchronized with the US image plane in real-time to help localize the target lesion and surrounding anatomical structures. We evaluated MRI-compatibility, targeting accuracy, and device setup duration for realistic clinical workflows, and system and workflow feasibility were demonstrated for a bovine liver phantom.

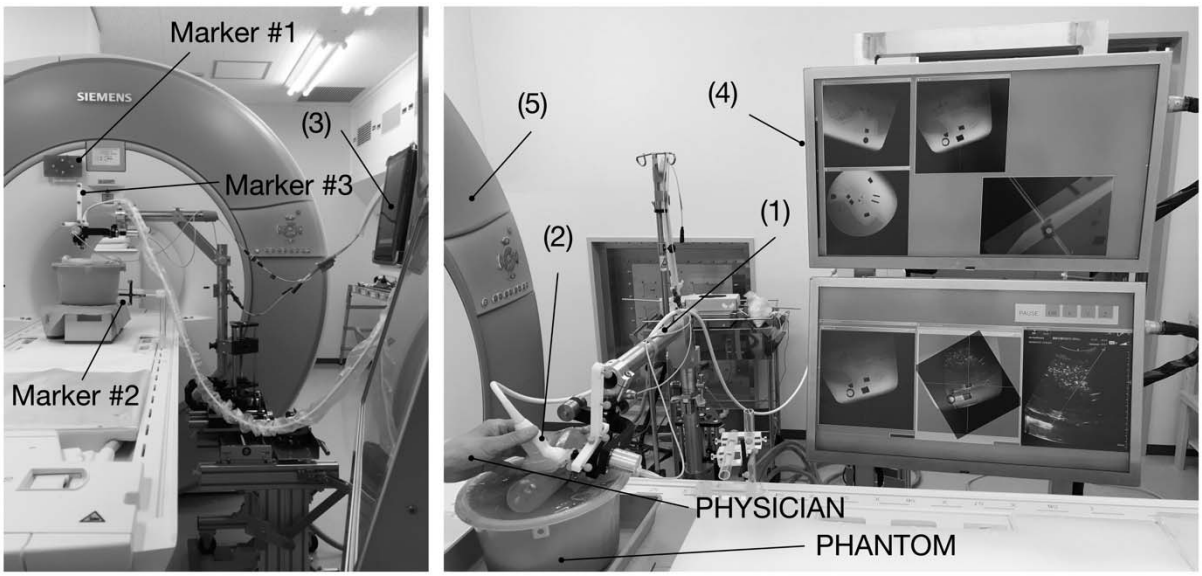

FIG. 1. Proposed navigation system based on simultaneous robotic and image guidance for interactive needle path planning and accurate needle placement: (1) needle manipulator; (2) ultrasound (US) probe; (3) US imaging scanner; (4) in-room monitors to display image guidance; (5) closed-bore MRI scanner; markers #1, #2, and #3 were used for the optical tracking sensor. A physician facing the needle manipulator across the patient table of the MRI scanner can interactively select an optimal needle path with the manipulator while observing the selected needle path candidate and surrounding structures (in this case for a phantom). Then, the physician can insert the needle along the needle guide while observing the insertion in US images with synchronized MR image plane on the monitors in real time.

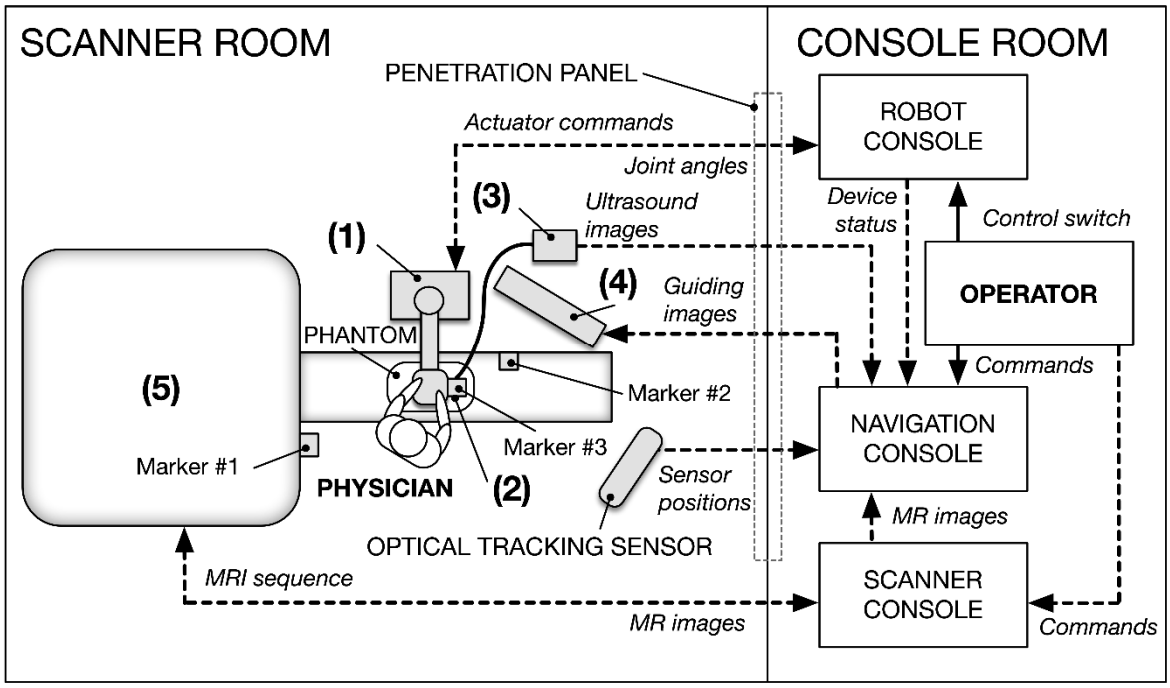

FIG. 2. The proposed simultaneous robotic and image guidance system: Components (1)–(5) are explained in Fig. 1. The system provides physician guidance in the scanner room with an operator in the console room next to the scanner room. The phantom in this diagram represents a patient's abdomen.

2. MATERIALS AND METHODS

2.A. System overview

The developed navigation system comprised a needle manipulator with US probe, in-room monitors, optical tracking sensor, and wide-bore 3 T MRI scanner (Magnetom Verio 3T, Siemens Healthcare, Erlangen, Germany) (Figs. 1 and 2). The hardware components were all placed in the scanner room and connected to robot and navigation consoles in the console room through a radio frequency filtered penetration panel (Riken Electromagnetic Compatibility Inc., Fukuoka, Japan) with waveguides. Customized image guidance software was installed on the navigation console.

Ultrasound imaging scanner. A portable diagnostic US imaging scanner (Venue 40, GE Healthcare) was integrated into the system to provide real-time image feedback during needle insertion. Sector (3S-SC, GE Healthcare) or convex (4C-SC) probe can be selected depending on the subject, and attached to the needle manipulator with 1.9 m cable. The US imaging scanner frame was replaced with a non-ferromagnetic frame (aluminum) to improve MRI safety.

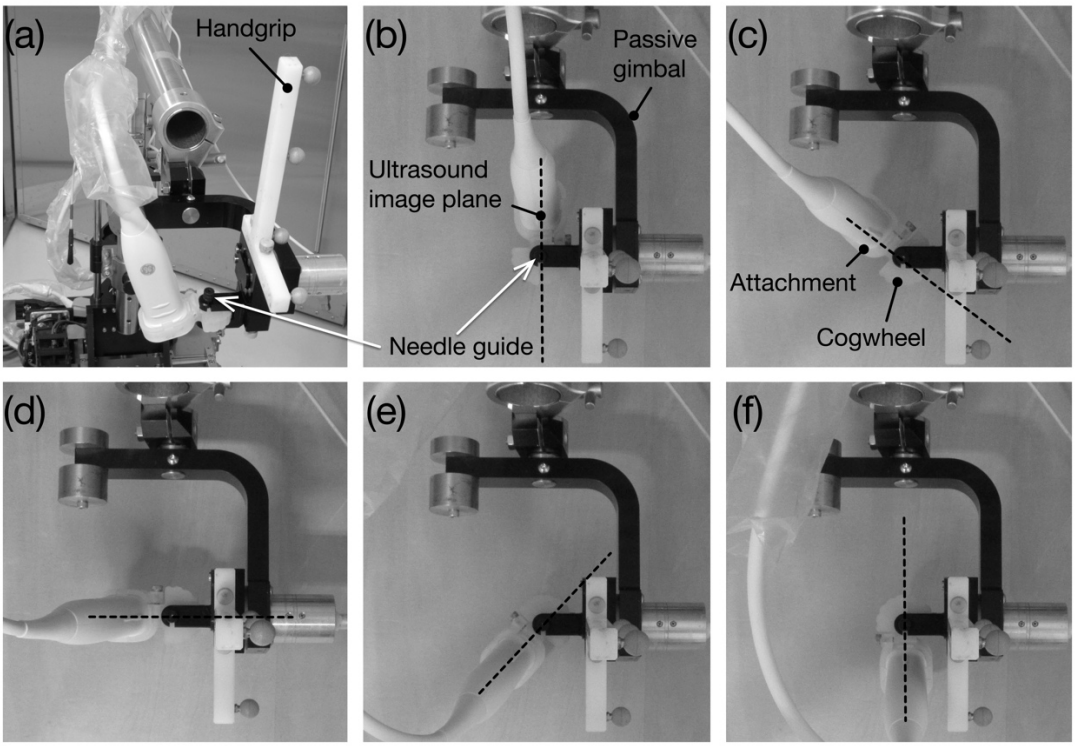

FIG. 3. Needle manipulator passive end effector: (a) overview, and (b)–(f) top views. The installed ultrasound (US) probe could be rotated 180° around the needle guide positioned at the intersection of the two passive gimbal rotational axes. The passive gimbal provided sufficient space for the US probe to be rotated. White solid arrows represent needle guide locations and dotted lines represent the US imaging plane.

Needle manipulator. The manipulator was a portable robotic arm comprising an end effector with passive gimbal and three-axis active linear base stage mounted on a four-wheel cart, where the linear base stage and cart were adapted from our previous works[15,16]. The range of motion for the linear base stage driven by non-magnetic ultrasonic motors was 230, 185, and 150 mm (width, depth, and height, respectively). The end effector was fixed to an L-shaped rigid arm mounted on the vertical axis of the linear base stage such that it was positioned above the patient table. The end effector comprised a needle guide and handgrip mounted on a two degrees of freedom (DOF) passive gimbal (Fig. 3). Each passive joint on the gimbal had a nonmagnetic optical rotary encoder (Prototype, Oshima Prototype

143 Engineering, Tokyo, Japan) to detect rotational angle. The needle path intersected the
144 crossing point of the two rotational axes. The needle guide included an unlock mechanism
145 with rotational collet to detach the inserted needle from the end effector. The US probe was
146 attached to the needle guide via a concentric cogwheel to facilitate adjusting the US scan
147 plane angle with respect to the needle path (Fig. 3). The US scan plane always coincided
148 with the needle insertion plane and the cogwheel could be rotated at 22.5° intervals. The US
149 probe could be detached from the needle guide.

150 The manipulator allowed a physician to tilt the needle guide freely via the handgrip[18]
151 while the base stage automatically adjusted the needle guide position using virtual remote
152 center of motion (Virtual RCM) control[19] to maintain the preset distance between the
153 needle guide and target, and keep the needle directed at the target, as shown elsewhere[15].
154 The ultrasonic motors and encoders can be turned on or off at the robot console
155 workstation, which also sends device status to the navigation console.

156 **Tracking sensor.** An optical tracking sensor (a Polaris Spectra position sensor with Extended
157 Pyramid Volume (EPV) [20], Northern Digital Inc., Ontario, Canada) was used to register the
158 MRI scanner, scanner patient table, and needle guide coordinate systems. Coordinate
159 registration was crucial, since the table and needle manipulator were not permanently fixed
160 to the MRI scanner. The tracking sensor was mounted on a 130 cm high four-wheeled cart.
161 Passive marker units for the sensor were attached to the MRI scanner housing (marker #1),
162 patient table (marker #2), and needle guide (marker #3) (Figs. 1 and 2) to provide locations
163 in the sensor coordinate system. The frame for marker #3 was the handgrip of the passive
164 end effector. The tracking sensor sends continuous data to the navigation console.

In-room monitors. MRI-compatible in-room monitors (Prototype, Takashima Seisakusho, Tokyo, Japan) displayed the image guidance graphical user interface (Fig. 4). The in-room monitors were flat-panel displays arranged vertically. The upper monitor displayed planning information, including three orthogonal MPR images perpendicular (transverse) and parallel (in-plane-0 and in-plane-90) to the needle path and a virtual bird's eye view of the three MPR image planes with a model of the target in the patient. The lower monitor displayed guidance information, including real-time US image, corresponding MPR image, and their fusion. The planned needle path was superimposed on the US image so the physician could monitor needle deviations from the planned path in real-time. Device status, including Virtual RCM mode status (on or off) and motion limit alerts for the three axis active linear base stage were also displayed.

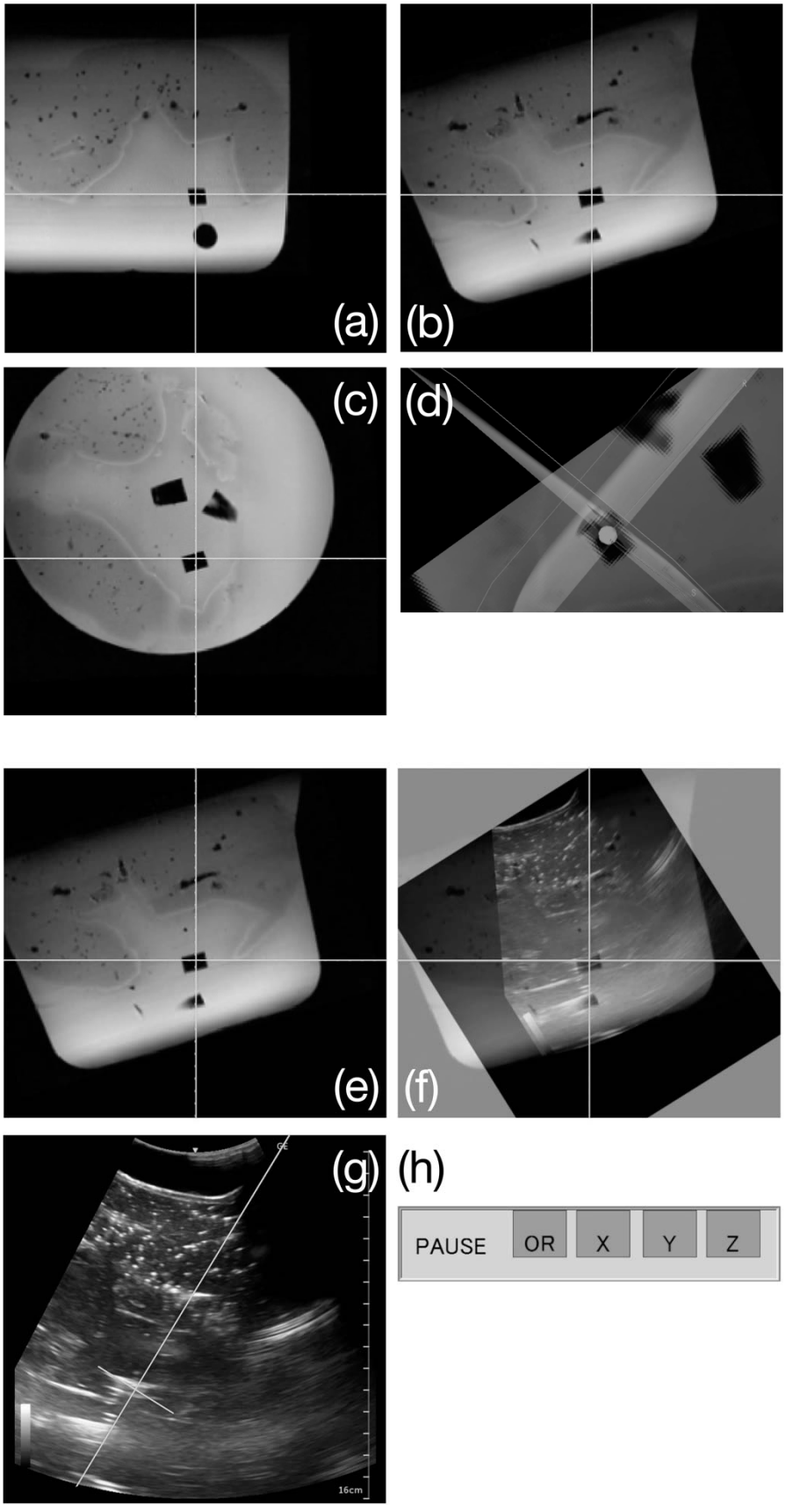

177

FIG. 4. Typical guiding images displayed on the (a)–(d) upper and (e)–(h) lower in-room monitors: (a) in-plane-0 multiplanar reconstruction (MPR) parallel to the needle path), where the vertical line represents the planned needle path, and its intersection with the solid horizontal line represents the target location; (b) in-plane-90 MPR; (c) MPR perpendicular to the needle path; (d) virtual bird's eye view; (e) corresponding MPR (in-plane-90 image in this figure; (f) ultrasound (US) image plane fused with the in-plane-90 image; (g) US image plane, where the long solid line represents the planned needle path, and the intersection with the short solid line represents the target location; (h) device status, i.e., (left to right) virtual remote center of motion mode status and motion limit alerts for the three axis active linear base stage.

Image guidance software. The image guidance software worked as an information hub for the entire system and provided following features: importing images from the MRI and US scanners, position and orientation of markers from the tracking sensor, and device status from the robot console, and visualizing them effectively with the procedure plan on the in-room monitors to navigate the procedure. Once the coordinate systems described above (*Tracking sensor)* were registered, the software could generate MPR images from MR images that were parallel and perpendicular to the US imaging plane. The software was developed in-house in C++ (Visual Studio 2008, Microsoft Corp., Redmond, WA) and installed on a navigation console workstation (Z800, 2.26 GHz dual quad-core Intel Xeon E5520 Processors, 24 GB 1,333 MHz DDR3 ECC RAM, NVIDIA Quadro FX 3800, HP Inc., Palo Alto, CA) with the Windows operating system (Windows 7 Professional 64-bit Service Pack 1, Microsoft Corp.). Ultrasound images were captured continuously by an image signal converter (DVI2USB 3.0, Epiphan Systems, Ottawa, Canada) and imported into the software using a free open-source computer vision library (OpenCV 2.4.10, Intel Corporation, Santa Clara, CA).

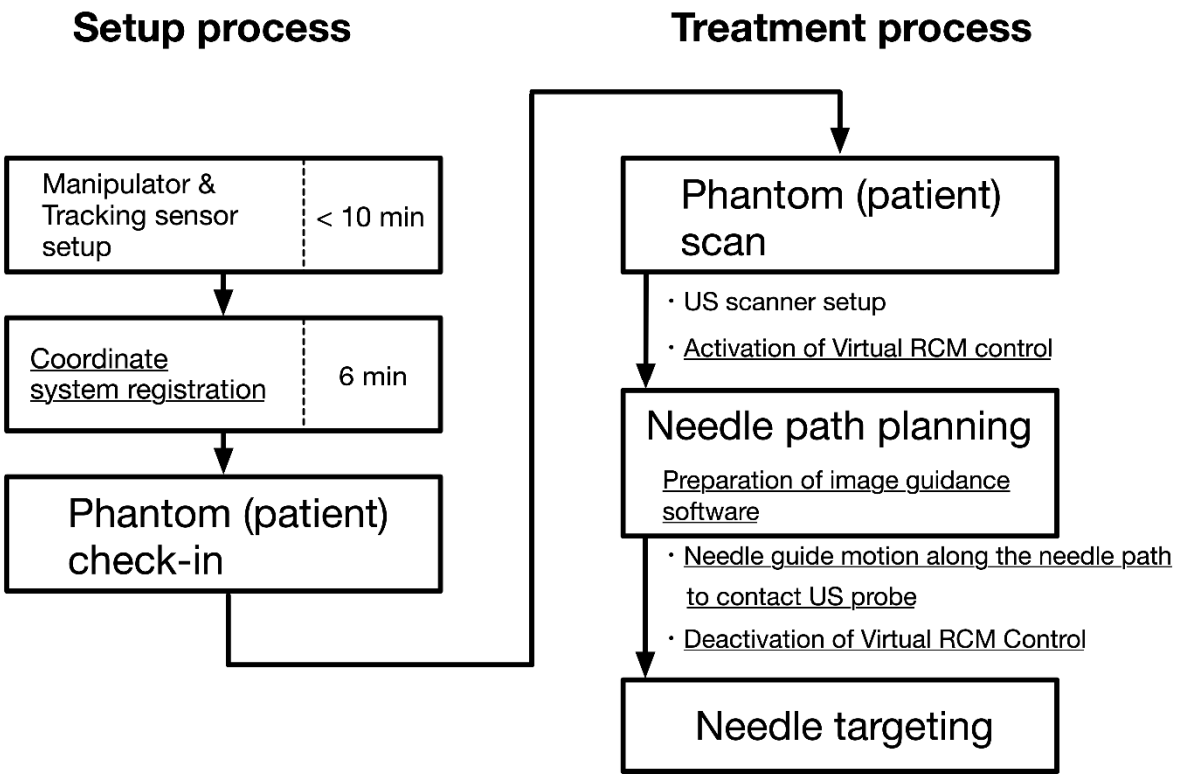

205

206 **FIG. 5.** Needle placement workflow using the proposed multi-modal image-guided
207 navigation system with needle manipulator. The setup process includes duration for each
208 phase, and tasks for the system operator in the console room are underlined.

209

210 **2.B. Workflow**

211 The workflow was designed based on our previous work[16] and included three phases in both
212 the setup and treatment processes, as shown in Fig. 5, including indicative setup component
213 durations. In the manipulator and tracking sensor setup phase, the manipulator was placed
214 next to the patient table without attaching the US probe. The actuator power supply cables
215 and the optical fiber cables of the encoders were connected to the robot console through
216 the waveguide on the penetration panel. A tracking sensor was located in the scanner room
217 such that all three markers were in the measurement volume. Registration with manipulator
218 calibration was performed by the operator, the registration transformation matrix was

loaded into the image guidance software, and then a phantom (patient) was placed on the table. The manipulator motor and encoder power supplies were turned off after setup completed.

The planning image was acquired in the scan phase. The US probe was not present in the MRI room during scanning to avoid electromagnetic (EM) interference with MRI. The patient table was then moved to the manipulator workspace. Targets were identified visually in the MR images on the scanner console, their coordinates were recorded, and the planning image was loaded into the image guidance software. One of the target coordinates was manually entered into the robot console, the motors and encoders were turned on, and the US probe was attached to the end effector, requiring less than one minute.

The manipulator was used for both path planning and needle targeting phases (Fig. 6). In the planning phase, the operator first set the preset distance on the image guidance software and then Virtual RCM control was activated. The physician stood on the lateral side of the patient table facing the manipulator and selected the optimal needle path by tilting the passive gimbal while observing guidance images on the upper monitor (Fig. 4). The needle guide was then moved along the selected needle path with the US probe making contact with the phantom (patient) surface through a water-filled rubber bag.

Virtual RCM control was turned off during the targeting phase to avoid unexpected actuation if the gimbal was accidentally rotated by contact with the phantom surface (patient's body). The physician then inserted the needle manually along the needle guide while observing the guidance images on the lower monitor (Fig. 4). The operator managed manipulator phase transitions on the robot console workstation, as shown in Fig. 5.

241

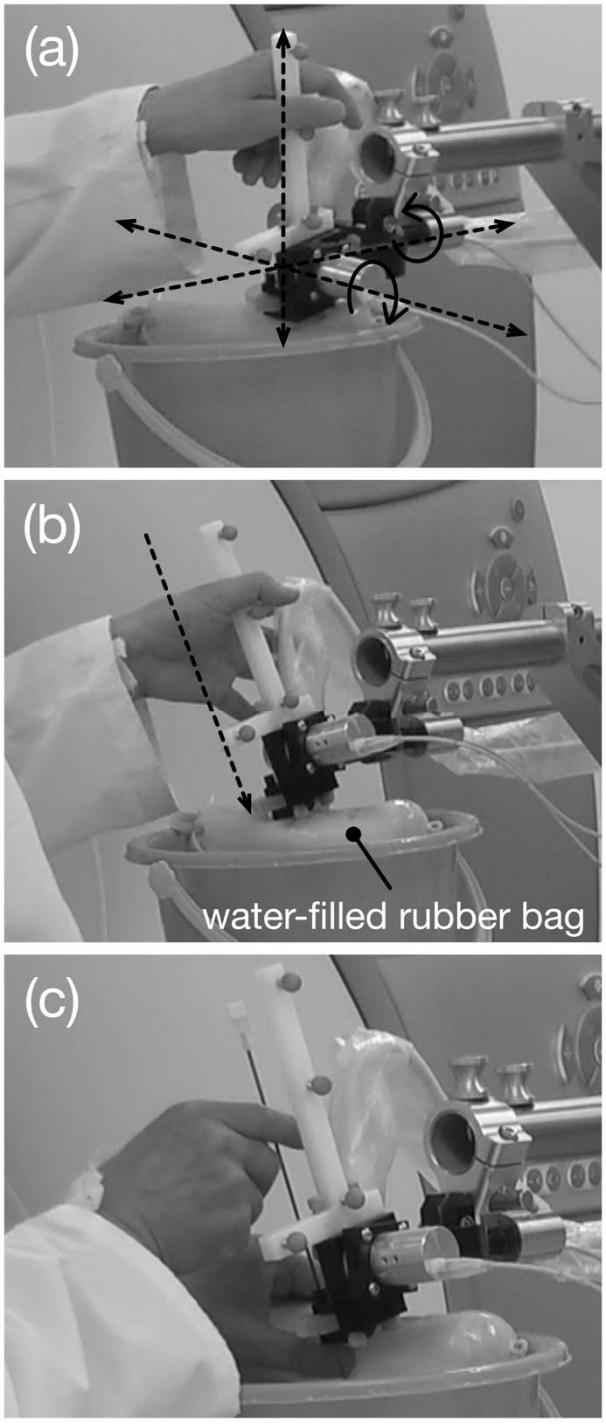

242

243 **FIG. 6.** Needle manipulator end effector in the interactive needle path planning and
244 targeting phases: (a) end effector manipulation in the planning phase, solid arrows
245 represent rotational motions by the physician facing the manipulator and dotted arrows
246 represent translational directions of the needle manipulator three axis active linear base
247 stage; (b) needle guide motion along the needle path to place the ultrasound probe in

248 contact with the water-filled rubber bag on the phantom; and (c) end effector in the
249 targeting phase, the physician inserts the needle along the needle guide.

250

251 **2.C. Feasibility using a phantom**

252 A mock procedure was performed with a phantom to qualitatively evaluate the proposed
253 navigation system and its workflow. The phantom was a 2.5 kg bovine liver submerged in
254 2% agar (010-15815 agar powder, Wako Pure Chemical Industries, Ltd., Osaka, Japan) mixed
255 with 0.25 mM Gd-DTPA in a plastic container, with small pieces of acrylic rods and tubes
256 distributed randomly as targets. A convex probe was used for US imaging. The scan phase
257 acquired a T1 weighted 3D image in the coronal plane with a Spine Matrix Coil using a 3D
258 fast acquisition low flip angle spoiled gradient echo sequence (TR/TE = 8.6/3.86 ms; flip
259 angle = 25°; acquisition matrix = 256×256; field of view (FOV) = 240×240 mm^2; slice
260 thickness = 2.5 mm). The preset distance was set to 150 mm to avoid contact between the
261 needle guide and phantom surface during path planning. After path planning, the water-
262 filled rubber bag was placed on the phantom surface with the appropriate amount of gel
263 (Aquasonic 100 Ultrasound Transmission Gel, 250 ml, Parker Laboratories, Inc., Fairfield, NJ)
264 (Fig. 6). The needle guide was moved along the needle path until the US probe had sufficient
265 contact with the rubber bag, and then a 20 cm 14 gauge MRI-compatible needle (Invivo,
266 Gainesville, FL) with a beveled tip was used. We performed the feasibility study five times
267 and recorded the time required for each setup (Fig. 5).

268 **2.D. Assessment of needle placement accuracy**

269 The targeting accuracy was assessed using an agar phantom made of 2% agar mixed with
270 0.25 mM Gd-DTPA in a plastic container. After scanning using the same imaging protocol
271 described above, we set the centroids of ten targets in the depth range 30–80 mm. We
272 designed five needle paths including a vertical path and four oblique paths for each target
273 by tilting the needle guide in a range of about ± 25°. The preset distance was set to 150 mm.
274 The needle was inserted using the needle guide while rotating the needle about its axis to
275 avoid needle deviation from the planned path. After insertion, the needle was retracted
276 while suctioning the agar on the needle path with a syringe attached to the needle top to
277 ensure the needle path was visible on the confirmation MR image. We performed 50 needle
278 targeting exercises for all ten targets. After targeting was completed, a confirmation image
279 was acquired using the same protocol as the planning image.

280 The confirmation image was assessed using 3D Slicer software[21] to measure the
281 distance between the needle path location and the target centroid orthogonal to the needle
282 path. In-plane distances for all paths were recorded as targeting errors and their average
283 and standard deviations were calculated.

284 **2.E. Impact on MR images**

285 We measured the signal to noise ratio (SNR) and distortion on MR images to assess the
286 proposed system impact. Six incremental system configurations were considered:

287 (1) Baseline: only the phantom and monitors were placed in the scanner room;

(2) Manipulator in Place: the manipulator and tracking sensor were placed in the scanner room but not connected to the robot console;
(3) Cable in Place: the cables were placed through the waveguide but not connected to the console;
(4) Cable Connected: the manipulator and tracking sensor were connected to the robot console;
(5) Manipulator Ready: the manipulator and tracking sensor were switched on; and
(6) System Ready: the US scanner was installed into the manipulator and connected to the navigation console.

We scanned an agar phantom for these assessments using two MRI pulse sequences: two-dimensional turbo spin echo (2D TSE) (TR/TE = 4,060/13 ms, acquisition matrix = 256×256; FOV = 150×150 mm^2; slice thickness = 5 mm; number of slices = 16), and three-dimensional gradient echo (3D GRE) (TR/TE = 60/8 ms; flip angle = 45°; acquisition matrix = 256×256; FOV = 150×150 mm^2, slice thickness = 5 mm; number of slices = 24). We used the difference image method for SNR measurement[22,23] and evaluated distortion by measuring phantom diameter on the image for each configuration.

3. RESULTS

3.A. Feasibility

The mock procedure was completed successfully. Figure 7 shows highlighted screenshots from the image guidance software displaying the needle. We visually confirmed that real-time US images visualized the needle path plane including the target, needle on the planned path, and surrounding soft tissue structures of the bovine liver. Alignment between the

planning MR and US images was visually assessed by observing the superimposed target and adjacent object outlines. Needle tip placement at the target was also confirmed on both images. Average times for manipulator and tracking sensor setup, coordinate system registration, and US scanner setup were 9.4 min, 5.7 min, and 51.4 s, respectively.

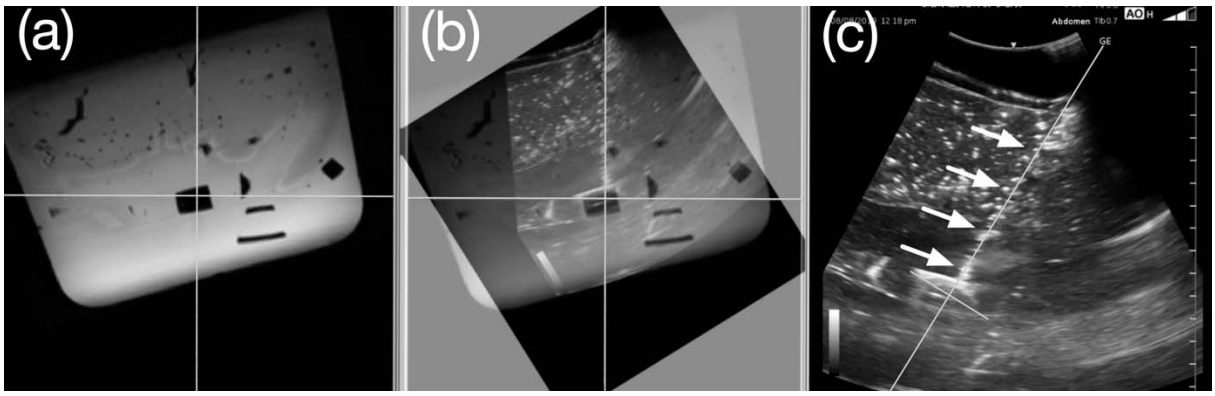

FIG. 7. Typical guiding image screenshots: (a) in-plane-90 planning MRI image, where the solid vertical line represents the planned needle path, and its intersection with the solid horizontal line represents the target location; (b) ultrasound (US) image plane fused with in-plane-90 image; (c) US image plane with inserted needle, where the long solid line represents the planned needle path, the intersection with the short solid line represents the target location, and solid arrows indicate the inserted needle.

3.B. Needle placement accuracy

Targeting error over fifty trials was 1.6 ± 0.6 mm (mean ± standard deviation), with maximum and minimum errors of 3.1 and 0.6 mm, respectively. Maximum and minimum needle path angles from the vertical line were 27.2° and -26.1°, respectively.

3.C. Impact on MR images

Figure 8 shows SNR for each configuration. SNR for 3D GRE was 46.9 for configuration 6 (see Section 2.E), which was the lowest SNR among all conditions; whereas SNR for 3D GRE was 82.5 for configuration 4, which was used for the planning image scan (Fig. 5). Distortion changes could not be confirmed in either sequence.

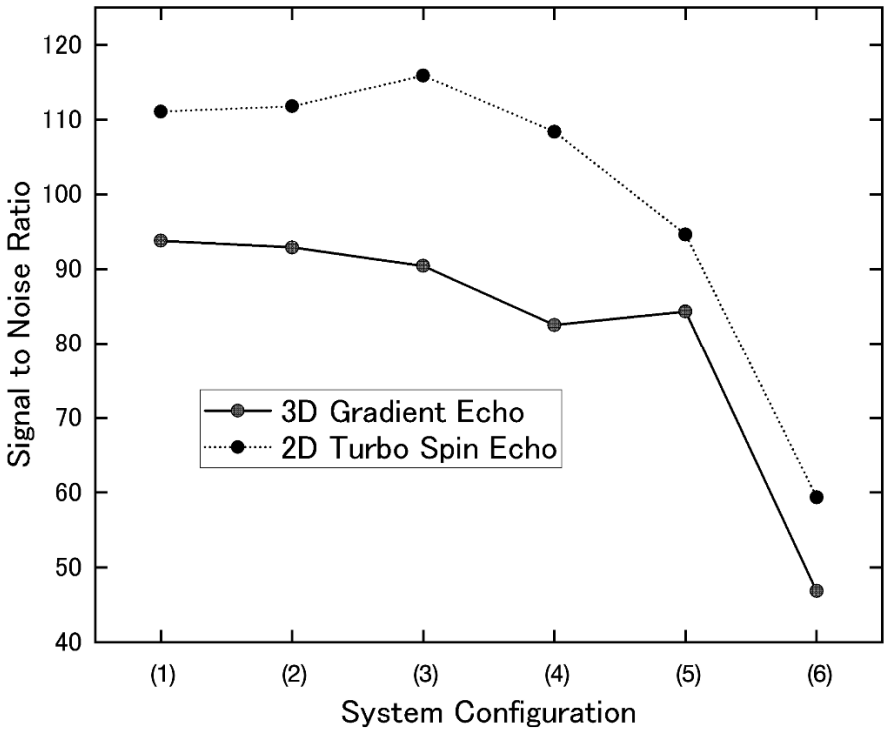

FIG. 8. Signal to noise ratio (SNR) for the system configurations detailed in Section 2.E.

4. DISCUSSION

We developed a multi-modal image-guided navigation system using a robotic needle manipulator. Cooperative physician–device interaction with MRI guidance helped the physician to follow the optimal needle path by fine tuning needle guide angles intuitively on the MRI scanner patient table. The proposed system also provided real-time fusion images on in-room displays after starting the needle targeting phase to help the physician confirm safe and accurate needle insertion, enabling needle placement with sufficient accuracy for liver tumor ablations[11]. Coordinate registration was completed before the phantom (patient) was placed on the table and hence did not disrupt treatment.

Several robotic assistance devices have been recently proposed for MRI-guided needle insertion applications[24,25], including patient[26–28] and scanner table[29,30] mounted robotic devices. Although patient mounted devices can be easily set up due to their small footprints, they must be placed at the correct incision site on the patient prior to the procedure, which may require repeated scanning and adjustments, prolonging procedure time since the patient must be moved in and out of the MRI scanner bore for each adjustment. However, the proposed method does not require this repeated process because the manipulator can adjust the entry point with translational DOFs in contrast with patient mounted devices. One limitation for the current proposed system is that the US probe was not specifically designed for use in MRI scanner rooms, and must be removed from the scanner room while the patient is being MRI scanned to ensure optimal MRI SNR (Fig. 8). However, clinical workflow disruption to attach or detach the US scanner was minimal, requiring approximately one minute.

Most MRI-guided needle insertion systems require confirmation MRI scan(s)[31] to determine insertion depth as the systems rely on low-resolution depth gauge[29] or scale on the inserted needle. However, the proposed system monitors needle insertion with real-time US imaging, synchronized MPR images, and the fused image helps determine needle depth, monitor tissues surrounding the needle path, and identify target organ shifts and needle deviations in real time.

Fusion image guidance combining MRI or CT with US imaging has been used clinically[32], including EM needle tracking for liver lesions[33–35]. Conventional US and contrast enhanced MRI image fusion improves liver lesion visibility, which would otherwise be invisible on conventional US images[36]. Image fusion using EM tracking requires plane and point registration to align MR and US images based on either external fiducial markers or internal anatomical landmarks. However, achieving acceptable accuracy matching these points or planes requires considerable training and experience[37]. Previous studies showed average registration error[38] of approximately 8 mm with best accuracy[39] of 1.9 ± 1.4 mm when US images were obtained immediately after CT acquisition under anesthesia[32]. The proposed navigation system and workflow eliminated training and experience requirements to achieve acceptable accuracy because MRI and US imaging coordinate systems are managed throughout the procedure by a single tracking sensor and markers attached to imaging scanners.

The proposed system leverages cooperative physician–device interaction to enable the physician to adjust needle guide angles directly in the scanner room. This physical input is more intuitive than control through a graphical user interface because the physician can maneuver the needle guide directly, without being distracted by needing to keep the needle

aligned with the target[8,40]. Adjusting the needle guide contact surface to obtain better US imaging is also very simple using the cogwheel.

Targeting error was equivalent to the authors' previous study using an open-configuration MRI scanner[15] even though the present system requires patient table motion in the workflow. Thus, the proposed system would provide sufficient needle placement accuracy for liver tumor ablation[11]. Real-time needle location feedback through US and fused images also allows the physician to immediately compensate for needle deviations, which are more likely when operating *in vivo*.

The water-filled rubber bag between the US probe and phantom (patient) surface ensures adequate contact between the probe and phantom surfaces, while allowing the physician to freely access the entry point on the patient table outside the MRI scanner bore. However, the rubber bag weight could risk potential surface (i.e., patient skin) deformation in clinical environments. One potential solution to minimize surface deformation would be to use commercially available sterile cover kits for the probe (CIV-Flex Covers, CIVCO Medical Solutions, Coralville, IA), which covers the US probe with a soft and durable flexible sheet for distortion-free imaging where the bottom part is filled with US transmission gel. The sheet could be fixed in the proper position with a band. A US probe covered with such a kit would enable adaptive contact between the probe and patient skin by deforming the filled gel, while avoiding deformation due to gel weight.

This study was limited to phantoms, which, although useful to evaluate clinical workflow feasibility, cannot incorporate several potentially confounding factors, such as target organ shifts and physical interactions between the needle and actual tissue. Future

403 animal studies will help assess system accuracy in the presence of those factors and
404 potentially highlight the proposed system's advantages.

405 **5. CONCLUSIONS**

406 We developed an MRI and US multi-modal image-guided navigation system using a robotic
407 needle manipulator, and demonstrated accurate needle insertion and seamless phase
408 transitions were achievable with the proposed system.

409 **ACKNOWLEDGMENTS**

410 This work was supported by JSPS KAKENHI (grants 26282145 and 18H01408), and NIH
411 (grants R01EB020667 and P41EB015898).

412 **CONFLICT OF INTEREST STATEMENT**

413 J.T. receives funding from Siemens Medical Solutions USA Inc. for a research project
414 unrelated to the present study. The other authors have no COI to report.

415

REFERENCES

1. Poon RT, Fan ST, Tsang FH, Wong J. Locoregional therapies for hepatocellular carcinoma: a critical review from the surgeon's perspective. *Ann Surg* 2002; 235(4):466–486.

2. Ido K, Isoda N, Sugano K. Microwave coagulation therapy for liver cancer : laparoscopic microwave coagulation. *Gastroenterology* 2001; 36(3):145–152.

3. Head HW, Dodd GD, 3rd. Thermal ablation for hepatocellular carcinoma. *Gastroenterology* 2004; 127(5 Suppl 1):S167–178.

4. Kahn T, Harth T, Kiwit JC, Schwarzmaier HJ, Wald C, Modder U. In vivo MRI thermometry using a phase-sensitive sequence: preliminary experience during MRI-guided laser-induced interstitial thermotherapy of brain tumors. *J Magn Reson Imaging* 1998; 8(1):160–164.

5. Lewin JS, Connell CF, Duerk JL, et al. Interactive MRI-guided radiofrequency interstitial thermal ablation of abdominal tumors: clinical trial for evaluation of safety and feasibility. *J Magn Reson Imaging* 1998; 8(1):40–47.

6. Morikawa S, Inubushi T, Kurumi Y, et al. Advanced computer assistance for magnetic resonance-guided microwave thermocoagulation of liver tumors. *Acad Radiol* 2003; 10(12):1442–1449.

7. Morikawa S, Inubushi T, Kurumi Y, et al. New assistive devices for MR-guided microwave thermocoagulation of liver tumors. *Acad Radiol* 2003; 10(2):180–188.

8. Sato K, Morikawa S, Inubushi T, et al. Alternate biplanar MR navigation for microwave ablation of liver tumors. *Magn Reson Med Sci* 2005; 4(2):89–94.

9. Schenck JF, Jolesz FA, Roemer PB, et al. Superconducting open-configuration MR imaging system for image-guided therapy. *Radiology.* 1995; 195(3):805–814.

10. Silverman SG, Collick BD, Figueira MR, et al. Interactive MR-guided biopsy in an open-configuration MR imaging system. *Radiology* 1995; 197(1):175–181.

11. Silverman SG, Tuncali K, Adams DF, et al. MR imaging-guided percutaneous cryotherapy of liver tumors: initial experience. *Radiology* 2000; 217(3):657–664.

12. Shiomi H, Naka S, Sato K, et al. Thoracoscopy-assisted magnetic resonance guided microwave coagulation therapy for hepatic tumors. *Am J Surg* 2008; 195(6):854–860.

13. Sonoda H, Shimizu T, Takebayashi K, et al. *Minimally invasive surgery using the open magnetic resonance imaging system combined with video-assisted thoracoscopic surgery for synchronous hepatic and pulmonary metastases from colorectal cancer: report of four cases. Surg Today* 2015; 45(5):652–658.

14. Murakami K, Naka S, Shiomi H, et al. Initial experiences with MR Image-guided laparoscopic microwave coagulation therapy for hepatic tumors. *Surg Today* 2015; 45(9):1173–1178.

15. Hata N, Tokuda J, Hurwitz S, Morikawa S. MRI-compatible manipulator with remote-center-of-motion control. *J Magn Reson Imaging* 2008; 27(5):1130–1138.

16. Morikawa S, Naka S, Murakami K, et al. Preliminary clinical experiences of a motorized manipulator for magnetic resonance image-guided microwave coagulation therapy of liver tumors. *Am J Surg* 2009; 198(3):340–347.

17. Morrison PR, Silverman SG, Tuncali K, Tatli S. MRI-guided cryotherapy. *J Magn Reson Imaging* 2008; 27(2):410–420.

18. Troccaz J, Delnondedieu Y. Semi-active guiding systems in surgery. A two-dof prototype of the passive arm with dynamic constraints (PADyC). *Mechatronics* 1996; 6(4):399–421.

19. Boctor EM, Webster RJ, 3rd, Mathieu H, Okamura AM, Fichtinger G. Virtual remote center of motion control for needle placement robots. *Comput Aided Surg* 2004; 9(5):175–183.

20. NDI Polaris position sensor. https://www.ndigital.com/medical/products/polaris-family/. Accessed January 22, 2019.

21. Fedorov A, Beichel R, Kalpathy-Cramer J, et al. 3D Slicer as an image computing platform for the Quantitative Imaging Network. *Magn Reson Imaging* 2012; 30(9):1323–1341.

22. Murphy BW, Carson PL, Ellis JH, Zhang YT, Hyde RJ, Chenevert TL. Signal-to-noise measures for magnetic resonance imagers. *Magn Reson Imaging* 1993; 11(3):425–428.

23. Firbank MJ, Coulthard A, Harrison RM, Williams ED. A comparison of two methods for measuring the signal to noise ratio on MR images. *Phys Med Biol* 1999; 44(12):N261–264.

24. Fisher T, Hamed A, Vartholomeos P, et al. Intraoperative magnetic resonance imaging-conditional robotic devices for therapy and diagnosis. *Proceedings of the Institution of Mechanical Engineers Part H, J Eng Med* 2014; 228(3):303–318.

25. Moche M, Zajonz D, Kahn T, Busse H. MRI-guided procedures in various regions of the body using a robotic assistance system in a closed-bore scanner: preliminary clinical experience and limitations. *J Magn Reson Imaging* 2010; 31(4):964–974.

26. Hata N, Song SE, Olubiyi O, et al. Body-mounted robotic instrument guide for image-guided cryotherapy of renal cancer. *Med Phys* 2016; 43(2):843–853.

27. Wu F, Torabi M, Yamada A, et al. An MRI Coil-Mounted Multi-Probe Robotic Positioner for Cryoablation. Paper presented at: 2013 ASME International Design Engineering Technical Conferences & Computer and Information in Engineering Conference IDETC/CIE; 4–7 Aug. 2013.

28. Song S, Tokuda J, Tuncali K, Yamada A, Torabi M, Hata N. Design evaluation of a double ring RCM mechanism for robotic needle guidance in MRI-guided liver interventions. Paper presented at: 2013 IEEE/RSJ International Conference on Intelligent Robots and Systems; 3–7 Nov. 2013.

29. Franco E, Ristic M, Rea M, Gedroyc WM. Robot-assistant for MRI-guided liver ablation: A pilot study. *Med Phys* 2016; 43(10):5347.

30. Stoianovici D, Jun C, Lim S, et al. Multi-Imager Compatible, MR Safe, Remote Center of Motion Needle-Guide Robot. *IEEE Trans Biomed Eng* 2018; 65(1):165–177.

31. Morikawa S, Haque H, naka S, et al. *An MR Image Navigation System for a Closed Bore Scanner with a Needle Insertion Manipulator.* Paper presented at: ACCAS 2013 9th Asian Conference on Computer-Aided Surgery; 16–19 Sep. 2013.

32. Ewertsen C, Saftoiu A, Gruionu LG, Karstrup S, Nielsen MB. Real-time image fusion involving diagnostic ultrasound. *AJR Am J Roentgenol* 2013; 200(3):W249–255.

33. Hakime A, Deschamps F, De Carvalho EG, Barah A, Auperin A, De Baere T. Electromagnetic-tracked biopsy under ultrasound guidance: preliminary results. *Cardiovas Intervent Radiol* 2012; 35(4):898–905.

34. Venkatesan AM, Kadoury S, Abi-Jaoudeh N, et al. Real-time FDG PET guidance during biopsies and radiofrequency ablation using multimodality fusion with electromagnetic navigation. *Radiology* 2011; 260(3):848–856.

35. Krucker J, Xu S, Venkatesan A, et al. Clinical utility of real-time fusion guidance for biopsy and ablation. *J Vasc Interv Radiol* 2011; 22(4):515–524.

36. Bo XW, Xu HX, Wang D, et al. Fusion imaging of contrast-enhanced ultrasound and contrast-enhanced CT or MRI before radiofrequency ablation for liver cancers. *Br J Radiol* 2016; 89(1067):20160379.

37. Wang S-Y. Real-Time Fusion Imaging of Liver Ultrasound. *J Med Ultrasound* 2017; 25(1):9–11.

38. Krücker J, Xu S, Glossop N, et al. Electromagnetic tracking for thermal ablation and biopsy guidance: clinical evaluation of spatial accuracy. J *Vasc Interv Radiol* 2007; 18(9):1141–1150.

39. Hakime A, Deschamps F, De Carvalho EG, Teriitehau C, Auperin A, De Baere T. Clinical evaluation of spatial accuracy of a fusion imaging technique combining previously

520 acquired computed tomography and real-time ultrasound for imaging of liver
521 metastases. *Cardiovasc Intervent Radiol* 2011; 34(2):338–344.

522 40. Kurumi Y, Tani T, Naka S, et al. MR-guided microwave ablation for malignancies. *Int J*
523 *Clin Oncol* 2007; 12(2):85–93.

524